Two-Dimensional Direct Simulation Monte Carlo (DSMC) of Reactive Neutral and Ion Flow in a High Density Plasma Reactor

Demetre J. Economou, Timothy J. Bartel, Richard S. Wise, and Dimitris P. Lymberopoulos

Abstract—**We present a two-dimensional direct simulation Monte Carlo (DSMC) study of the rarefied reactive flow of neutrals and ions in a low pressure inductively coupled plasma reactor. The spatially-dependent rate coefficients of electron impact reactions and the electrostatic field were obtained from a fluid plasma simulation. Neutral and ion etching of polysilicon with chlorine gas was studied with emphasis on the reaction uniformity along the wafer. Substantial gradients in total gas density were observed across the reactor invalidating the commonly made assumption of constant gas density. The flow was nonequilibrium with differences in the species translational temperatures, and 100 K temperature jumps near the walls. When etching was limited by ions the etch rate was highest at the wafer center. When etching was limited by neutrals, the etch rate was highest at the wafer edge. In such case, the etch uniformity changed significantly depending on the reactivity of the ring surrounding the wafer. The ion angular distribution was several degrees off normal and it was different at the wafer edge compared to the rest of the wafer.**

I. Introduction

Low pressure (< 50 mtorr) high density (> 10^{11} cm^{-3}) plasma (HDP) sources are being investigated for etching and deposition of thin films used in microelectronic device fabrication [1]–[3]. Examples include electron cyclotron resonance (ECR), inductively coupled plasma (ICP), helicon, and helical resonator sources. Low pressure allows for more directional ion bombardment and, hopefully, better plasma uniformity and reduced contamination. High plasma density is then required to achieve reaction rates comparable to those in more conventional high pressure (100 s of mtorr) plasma reactors. One of the central goals of HDP sources is to achieve uniform fluxes of neutral radicals and ions over large diameter (> 200 mm) wafers. In addition, the energy and angular distribution of ions must be controlled. The flux uniformity, energy and angular distributions depend on a complicated manner on reactor geometry, operating conditions, and any externally applied magnetic fields.

Mathematical models of plasma generation and transport can be useful for improving our understanding of reactive gas plasmas and for investigating the effect of reactor design and operating conditions on plasma uniformity over semiconductor wafers. Models of HDP sources range from 0-D (well-mixed) descriptions focusing on plasma chemistry, to 2-D self-consistent simulations [4]–[7]. The latter use the fluid approximation [4], [5], or some kind of hybrid approach [6], [7]. Analytic models have also been proposed [8]. Fluid models need to be scrutinized as the local Knudsen number $\mathrm{Kn} = \lambda/L > 0.1$, where λ is the mean free path of the plasma species, and L is a characteristic length scale of the reactor. A benchmark comparison of fluid models with fully kinetic particle-in-cell with Monte Carlo Collisions (PIC/MCC) simulations showed that the fluid models can yield results which are surprisingly close to those of PIC/MCC even under conditions for which $\lambda > 0.1L$ [9]. PIC-MCC simulations have been employed to study plasma reactor dynamics by resolving the short time scale (<ns) of electron motion [10], [11]; these simulations do not consider neutral transport and reaction which occurs on a much longer time scale (100 s of ms). Compared to fluid simulations, kinetic simulations provide much additional information about the glow discharge, including the energy and angular distributions of ions and neutrals bombarding the wafer. Such information is critical for use as input to microscopic feature evolution simulators to predict the final shape of patterns etched into the wafer. Also, kinetic simulations provide information about the species (electrons, ions, neutrals) velocity distribution function (VDF). This way one does not need to invoke approximations about the VDF, especially the electron VDF which is important for determining the electron-impact reaction rate coefficients (ionization, dissociation, etc.). Table I compares the direct simulation Monte Carlo (DSMC) method, a kinetic simulation used in the present work, with a fluid simulation.

DSMC has been employed extensively to study the rarefied gas flows encountered in aerodynamics [12]–[14]. Recently, DSMC has been applied to problems related to the microelectronic device fabrication. However, only neutral flow has been considered by DSMC so far. Reference [15] modeled rarefied neutral gas transport in a low pressure chemical vapor deposition (LPCVD) reactor. Neutral atom transport in a sputtering chamber has been studied by [16]-[19] used DSMC to simulate neutral flow in an inert (argon) glow discharge sustained in an ECR chamber. The ionization rate was obtained from a plasma fluid simulation. The authors did not follow ion transport with DSMC and they did not include bulk gas flow (a stagnant cell was assumed) or chemistry (no etching).

Manuscript received October 13, 1994; revised December 21, 1994. This work was supported in part by Sandia National Laboratories under a CRADA with SEMATECH, in part by the National Science Foundation under Grant CTS-9216023, and in part by The Welch Foundation.

D. J. Economou, R. S. Wise, and D. P. Lymberopoulos are with the Plasma Processing Laboratory, Department of Chemical Engineering, University of Houston, Houston, TX 77204-4792 USA.

T. Bartel is with Sandia National Laboratories, Albuquerque, NM 87185-0826 USA.

IEEE Log Number 9412956.

0093-3813/95$04.00 © 1995 IEEE

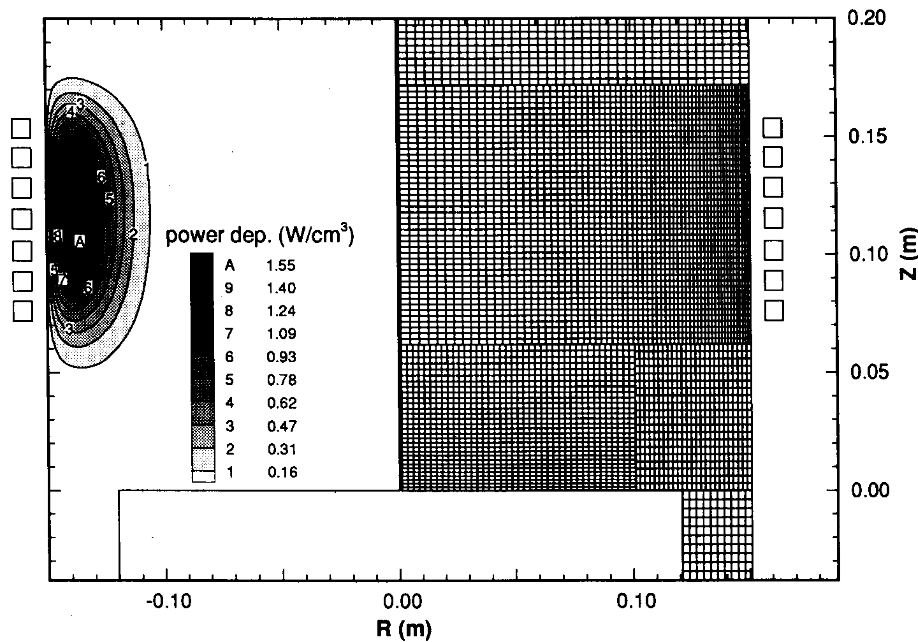

Fig. 1. (Left) Power deposition profile. Most of the power is deposited within the skin depth. (Right) Structure of the DSMC cells.

TABLE I
DSMC VERSUS FLUID SIMULATION

DSMC	Fluid
Particle-based kinetic simulation	Finite element solution of partial differential equations of continuity
Provides species distribution functions as output (including energy and angular distributions at wafer)	Requires species distribution functions as input.
More information about discharge (molecular level information)	Less information about discharge (averages over distribution function)
Can handle arbitrary 3-D geometries, complex boundary conditions	Boundary conditions may be difficult to specify
Robust (there is always a solution)	Convergence is not guaranteed
Long CPU time (Massively Parallel Supercomputer)	Short CPU time (Workstation)

In this paper, we present a two-dimensional kinetic simulation of the *neutral and ion* flow in a HDP reactor using the DSMC method. This is a reactive flow simulation of polysilicon etching with a chlorine plasma. The electrons are not followed by DSMC; instead a fluid plasma model is used to provide the space-dependent rate coefficients for electron-impact reactions and the space charge field. The power deposition into the discharge is calculated by solving Maxwell's equations and the self-consistent electrostatic fields are computed from the Poisson's equation. The ions and radicals generated by electron impact and by plasma or surface reactions are followed by DSMC. This can be seen as a hybrid simulation in which some species are treated as fluid and others as particles. For our purpose, we thought that it is important to treat the heavy species kinetically, since it is these species which perform chemistry on the wafer. Treating all species (including electrons) by DSMC is conceptually straightforward, but special care has to be exercised to decouple the disparate time scales of electron and heavy species transport. To our knowledge, this is the first DSMC simulation of neutral and ion transport in a glow discharge plasma. Preliminary results were presented before [20].

II. DSMC SIMULATION

A. Problem Statement

The inductively coupled plasma source studied is shown schematically in Fig. 1. The plasma is generated by a solenoidal coil wrapped around the cylindrical quartz wall of the reactor. The coil is excited by a 13.56 MHz power supply which is used to control the plasma density, and hence the ion flux to the wafer. The number and location of the coil turns is a design variable, although a fixed coil configuration was used for the results reported in this paper. The substrate electrode holding the wafer can be biased by an independent RF power supply to control the energy of ions bombarding the wafer. This independent control of ion bombardment flux and energy is a great advantage of HDP sources.

A chlorine plasma etching polysilicon was simulated in this reactor. The task of the simulation is the following: for given reactor and coil design, and given operating conditions (pressure, frequency, power, flow rate, wall temperature, etc.) determine the etch rate and uniformity across the wafer, as well as important internal plasma variables such as species density, and energy and angular distribution of neutrals and ions bombarding the wafer.

Microscopic feature evolution is outside the scope of this paper. However, the energy and angular distribution of ions and neutrals bombarding the wafer may be used as input to a feature evolution model to calculate the final wall profiles of patterns etched into the wafer. Actually, the problems of

TABLE II
COLLISION PROCESSES IN CHLORINE DISCHARGE INCLUDED IN DSMC SIMULATION

No.	Process	Reaction	Threshold (eV)
	Electron Impact Reactions*		
1	Dissociative Excitation	$Cl_2 + e \rightarrow Cl_2^*(C^1\Pi) + e \rightarrow 2Cl + e$	3.12
2	Molecular Ionization	$Cl_2 + e \rightarrow Cl_2^+ + 2e$	11.47
3	Atomic Ionization	$Cl + e \rightarrow Cl^+ + 2e$	12.99
4	Dissociative Attachment	$Cl_2 + e \rightarrow Cl_2^{-*} \rightarrow Cl^- + Cl$	0.0
5	Electron-Ion Neutralization	$e + Cl_2^+ \rightarrow 2Cl$	0.0
6	Detachment	$e + Cl^- \rightarrow 2e + Cl$	3.61
	Other Reactions		
7	Ion-Ion Recombination	$Cl_2^+ + Cl^- \rightarrow 3\ Cl$	
8	Ion-Ion Recombination	$Cl^+ + Cl^- \rightarrow 2Cl$	
9	Charge Exchange	$Cl^+ + Cl \rightarrow Cl + Cl^+$	
		$Cl_2^+ + Cl_2 \rightarrow Cl_2 + Cl_2^+$	
10	Etching	$2Cl + Si \rightarrow SiCl_2$	
		$2Cl^+ + Si \rightarrow SiCl_2$	
		$Cl_2^+ + Si \rightarrow SiCl_2$	
11	Wall Recombination	$2Cl + Wall \rightarrow Cl_2 + Wall$	

* Other electron impact reactions were also included in the electron fluid simulation. For a more complete list see Ref. 25.

reactor and feature evolution simulation may be coupled by the etch products evolved into the plasma which may well alter the plasma chemistry.

The electron-heavy particle reactions considered in this work are shown in Table II. Six heavy species and their reactions were followed by DSMC: Cl, Cl^+, Cl^-, Cl_2, Cl_2^+, and $SiCl_2$. The latter was thought to be an "average" reaction product.

B. The DSMC Method

DSMC is a method for the direct simulation of rarefied gas flows [12]. The flow domain is divided in a number of cells. The cell size is determined by the local mean free path λ; a size $\sim\lambda/3$ is typically recommended. The actual flow field is simulated using a number of simulated molecules (some 10^7 molecules are typical for runs on massively parallel supercomputers). In this context, the word molecules includes all kinds of species such as radicals, ions etc., as well as molecules. The species type, spatial coordinates, velocity components, internal energy, and weight factor of each simulated molecule are stored in the computer. The weight factor is the number of real molecules represented by each simulated molecule. As the molecules move through the reactor, molecules collide with one another and with the walls of the container. Feed molecules may be introduced at specified inlet port locations, and molecules may be removed from the simulation because of chemical reactions (in which case their identity changes) or through the pumping ports.

The basic premise of DSMC is that the motion of simulated molecules can be decoupled from their collisions over a time step. The size of the time step is selected to be a small fraction of the mean collision time, or a fraction of the transit time of a molecule through a cell. During the motion phase, molecules move in free flight according to their starting velocity and the forces acting on the molecules (for example electric field force on ionized species). During this phase, molecules may cross cell boundaries, collide with walls, or exit the flow field. During the collision phase, collision pairs are selected from within each cell *regardless of the position* of the molecules within the cell. It is imperative that the collision frequency occurring in the actual flow field is simulated correctly. The no-time-counter (NTC) technique [12], [13], was employed to handle collisions. This technique does not have the disadvantages of the older time counter (TC) method, while maintaining computational efficiency, i.e., the simulation time is proportional to the number of molecules. This is a great advantage of DSMC as compared to other particle simulation methods such as molecular dynamics. One should note that DSMC is limited to binary collisions. This does not pose a problem for the low pressure simulations of interest. Also, DSMC should be distinguished from the "test particle" Monte Carlo method. The latter is used to track the motion of a test molecule through a flow field established by some other means (e.g., a fluid simulation). The test molecule does not influence that flow field. Statistics are collected by following the trajectories of many test molecules. In DSMC, each and every molecule can influence the flow of the other molecules; i.e., the flow field is the result of the collective behavior of all molecules.

Because of the axisymmetric nature of the problem only two position coordinates (r, z) of each simulated molecule need be retained. However, collisions were handled as three dimensional events. The molecular model used was the variable hard sphere (VHS) model [12]. According to this model, the collision cross section σ_{ij} depends on the relative speed of the colliding partners E_c as

$$\sigma_{ij} = A_{ij} E_c^{-\omega} \tag{1}$$

where A_{ij} is a constant and $\omega = s - 0.5$, s being the exponent of the dependence of the coefficient of viscosity on temperature. The chief advantage of the VHS model is that, although the collision diameter is allowed to vary with relative speed (hence collisions do not occur with the same velocity dependence as hard sphere collisions), when a collision does occur, the post-collision velocity components are computed as if it were a hard sphere collision; i.e., isotropic scattering in the center of mass frame of reference.

The DSMC code has the capability of handling rotational and vibrational energies, and internal energy exchange in collisions by using the phenomenological [21] model, given the number of internal degrees of freedom of each species. The computer code includes many advanced features such as:

1) automatic cell structure generation for arbitrary geometries.
2) different regions of the computational domain can have a different time step and weight factor.
3) dynamically adjustable species weight factors. This is important when trace species are present.
4) cell weighting factors. This feature is useful for axisymmetric simulations in which cells around the reactor axis have much smaller volume (for roughly constant "grid" spacing), and can contain much fewer molecules compared to cells around the periphery, and
5) dynamic load balancing, a feature useful for achieving optimum speedup on massively parallel supercomputers with hundreds to thousands of processors. The purpose is to balance the work each processor has to carry out,

so that some processors do not remain idle waiting for others to finish their work.

C. Initial and Boundary Conditions

Two kinds of initial conditions were used. One is for simulations starting "afresh," some 5×10^5–2×10^6 molecules were loaded with equal probability of being placed in any volume element of the computational domain. The initial velocity components of the molecules were selected from a Maxwellian distribution with temperature 300 K. The second is for simulations from a "restart" file, the results of a previous run with similar operating parameters was used as initial condition. This method allowed for quicker approach to steady flow.

In practical systems, the gas is injected through small portholes (< 1 mm in diameter) distributed around the reactor periphery or on the reactor roof. This is clearly a 3-D arrangement. In order to reduce the problem to an axisymmetric flow, the gas was assumed to be injected through a slit forming a ring around the quartz cylinder. Because of the small size of the portholes, the pressure inside the feed gas lines is high enough for the flow to be "choked" as the gas expands into the low pressure reactor. Hence gas injection was modeled as an axisymmetric point source with sonic speed at the reactor inlet and 256 K inlet temperature of the expanding gas (corresponding to pure Cl_2 injection). The inward (in the $-r$ direction) component of the species velocity was selected in proportion to the distribution function $h(v) = (v + c_s)\{\exp - (av)^2\}$ where c_s is the local speed of sound, and $a = \sqrt{[M_{Cl_2}/(2RT_{gi})]}$, with M_{Cl_2} being the molecular weight of Cl_2, R the universal gas constant, and T_{gi} the inlet gas temperature. The other two velocity components were selected from a Maxwellian at 256 K. The acceptance-rejection method [12] was used to sample $h(v)$. Only negative values of v were allowed from the definition of the coordinate system. The incoming flux was set by the inlet mass flow rate of 200 sccm (1 sccm = $4.48\backslash 10^{17}$molecules/s).

The wafer temperature was set at 375 K; all other surfaces were set at 325 K. The outlet boundary condition was modeled based on the pumping speed at the reactor exit. A "pumping region" was defined at the exit (not shown in Fig. 1), and randomly selected molecules were removed from this region according to the pumping speed and the size of the time step. A pressure "control" loop was also implemented to dynamically adjust the pumping speed to achieve the desired pressure for given inlet flow rate. The pressure control point was selected to be at ($z = 0$, $r = 13.5$ cm).

D. Surface Chemistry

Chemistry on surfaces other than the wafer was specified as follows: Cl atoms recombine on the surface to form molecular chlorine with probability $\gamma = 0.0082$ [22] or $\gamma = 0.1$. Complete thermal accommodation with the surface was assumed for all impinging neutral species. Ionic species were also accommodated and fully neutralized at the surface. Two different extreme chemistries were considered on the wafer surface: 1) Cl atoms etch the wafer with probability $\gamma = 0.1$ to produce $SiCl_2$. The rest of the species interact with the wafer as with the nonwafer surfaces. This case will be referred to as *neutral etching*. This case may be a better approximation for heavily doped n-type polysilicon. 2) The atomic and molecular chlorine ions etch the wafer to produce $SiCl_2$ with probability 0.5. This case will be referred to as *ion etching*. This case is a better approximation for undoped polysilicon and assumes that the surface is fully chlorinated even at the low pressure of operation of the HDP source [23]. We realize that the reaction probability of impinging ions depends on their energy; a chemical sputtering yield Y (silicon atoms removed per ion) of the form

$$Y = A(E_+ - E_{th})^{0.5} \tag{2}$$

has been postulated [24], where A is a constant depending on the material and chemical system, E_+ is the ion energy, and E_{th} is a threshold energy. In the results reported below an "average" reaction probability (= 0.5) was assumed. Incorporating an energy-dependent reaction probability is straightforward in DSMC and will be added in the future. Etching and surface recombination reactions are shown schematically in Table II as reactions 10 and 11, respectively.

E. Gas-Phase Chemistry

The electron-impact processes included as source terms in the DSMC simulation are shown as reactions (1)–(6) in Table II. Other electron-impact reactions (e.g., electronic excitations, momentum transfer) which were included in the plasma fluid simulation are not shown in Table II. A complete set of reactions can be found in [25]. Energy released in exothermic reactions was distributed randomly in the newly created species as excess translational energy. For example, dissociation of molecular chlorine produces two chlorine atoms with 0.6 eV excess energy (Frank-Condon effect). Similarly, dissociative attachment (reaction 4) is exothermic by 3.61 eV, and dissociative recombination reactions 7 and 8 are exothermic by 7.86 eV and 9.38 eV, respectively. Charge exchange reactions between heavy particles were also considered as shown by reaction 9 in Table II. Due to lack of detailed data, the cross section was taken equal to 1.2×10^{-18} m^2 for both charge exchange reactions.

F. Execution of the Simulation

Calculations were performed on a 1024-node nCUBE-2 massively parallel supercomputer. Typically some 5×10^5–2×10^6 molecules were used, which on the average resulted in 100–400 molecules per DSMC cell. The simulation progressed for 5×10^4–2×10^5 time steps, each with a step size of 10^{-6} s for neutral motion. Subcycling was used for ion motion to better capture the ion trajectories. In the bulk of the plasma the ion time step was 3 times smaller than that of neutrals; near the walls it was 45 times smaller since strong electric field gradients are confined near the wall. Separate calculations with neutrals only have shown a speed up of 40X over a single Cray Y/MP processor using a 1024-node nCUBE-2, and a speed up of 100X over a single Cray Y/MP processor using a 512-node Intel Paragon. This tremendous speed up allows calculations which were previously thought impractical to be performed in several hours. Thus, parametric investigations of the reactor are feasible.

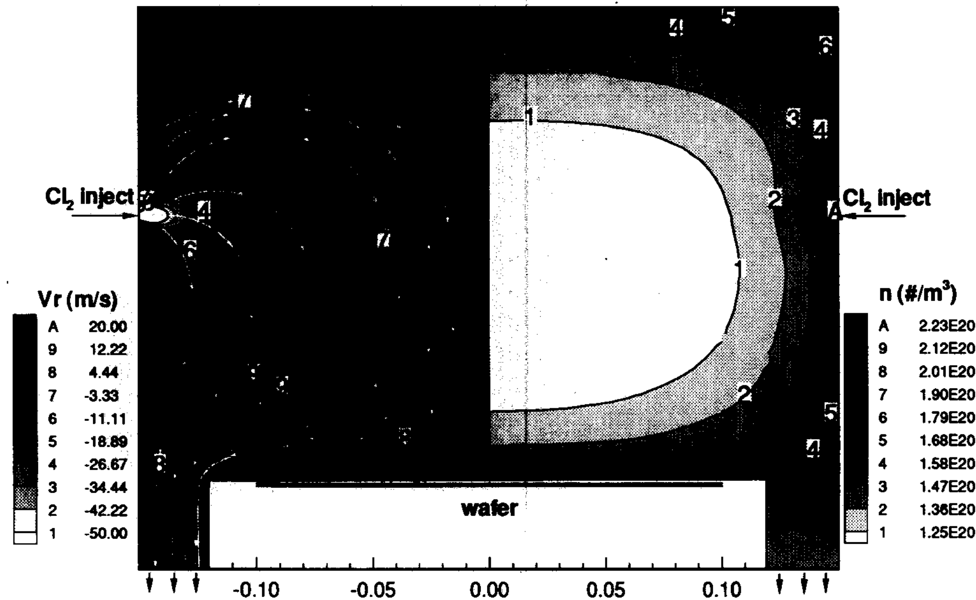

Fig. 2. (Left) Flow field showing representative streamlines; gray scale shows the radial component of the gas velocity; the plume expansion at the gas inlet is clearly evident. (Right) Total number density in the reactor, N. Note, the local maximum in N around the wafer periphery. Both sides of the figure are for the case of neutral etching and the recombination probability of Cl atoms on all nonwafer walls is $\gamma = 0.0082$.

After an initial "transient," molecular quantities were sampled every time step and used to update statistical sums representing macroscopic properties of the flow (pressure, temperature, flow velocities etc.). Time evolution simulations are also possible by ensemble averaging the results of many separate simulations. However, due to the hybrid nature of our approach (fluid electrons, particle neutrals and ions), the plasma transients can't be captured; only the final steady-state solution can be obtained by our simulation.

III. Results and Discussion

In the present work, 5225 cells were used in a structure shown in Fig. 1 (right). Cells are grouped in regions, each of which is distinguished by a special "boundary condition" of the system. For example, a region having the wafer as one of its boundaries, or a region used for simulating pumping action (not shown in Fig. 1). A separate grid (not shown) was used for solving the Poisson equation to obtain the electrostatic fields. Since the sheath thickness in high density plasmas is only 100 s of μ thick, a finite element grid spacing of 35 μ was used near walls to resolve the sheath. Fig. 1 (Left) shows the power deposited in the plasma by the electromagnetic (EM) field. The power deposition peaks near the induction coils. The EM field is shielded by the high density plasma. The penetration depth of the field (~few cm) is of the order of the local skin depth. The ionization rate (not shown) was nonuniform but not as localized as the power deposition. This is because, at these low operating pressures, thermal conduction heats the electrons further away from the power deposition zone. The dissociation rate was less nonuniform as compared to ionization, since the threshold ("activation") energy for dissociation of molecular chlorine (3.12 eV) is much lower than that for ionization of atomic (12.99 eV) and molecular (11.47 eV) chlorine. Fig. 1 also shows the center $(z, r) = (0,0)$ of the coordinate system used, which coincides with the wafer center.

Figs. 2–4 shown below are for the case of neutral etching. The same general characteristics were observed for the case of ion etching as well. Fig. 2 (Left) shows representative flow streamlines and a gray scale of the *radial component* of the average flow velocity. The plume due to the incoming feed gas is clearly seen. The gas at the upper part of the reactor is relatively stagnant. The total number density in the reactor (all neutrals and ions) is shown in Fig. 2 (Right). The ion densities are too low (see below) to make any significant contribution to the total density. The total number density is highest ($>2.2 \times 10^{20}$ m^{-3}) at the point of introduction of the feed gas ($z = 0.112$ m, $r = 0.15$ m) and lowest ($<1.25 \times 10^{20}$ m^{-3}) around the reactor center (an even lower number density was obtained further down in the exhaust port which is not shown in Fig. 2). Clearly, there is a significant difference in number density between the "bulk" of the plasma and the walls. This is due to "ion pumping" and gas heating. Neutrals are ionized in the bulk, and the ions are propelled by the space charge field towards the walls where they recombine with electrons turning back into neutrals. This ion pumping results in a higher neutral density near the walls. In addition, the gas is hottest (500–600 K) near the center of the reactor, which also contributes to lower the number density there. The total number density along the wafer surface is quite uniform, except for the wafer edge, where a slight local build up is observed. This is because Cl atoms (the major species in the system, see Fig. 3), are not consumed as fast on the ring surrounding the wafer compared to the wafer itself. (a wall recombination probability of $\gamma = 0.0082$ was used for all nonwafer walls in Fig. 2.); and there is a decrease in the number of moles upon Cl reaction on the wafer (two Cl atoms result in one product molecule $SiCl_2$).

Fig. 3 shows the atomic chlorine number density in the reactor. The left side corresponds to a Cl reaction (recombination) probability on all nonwafer surfaces of $\gamma = 0.0082$. The high

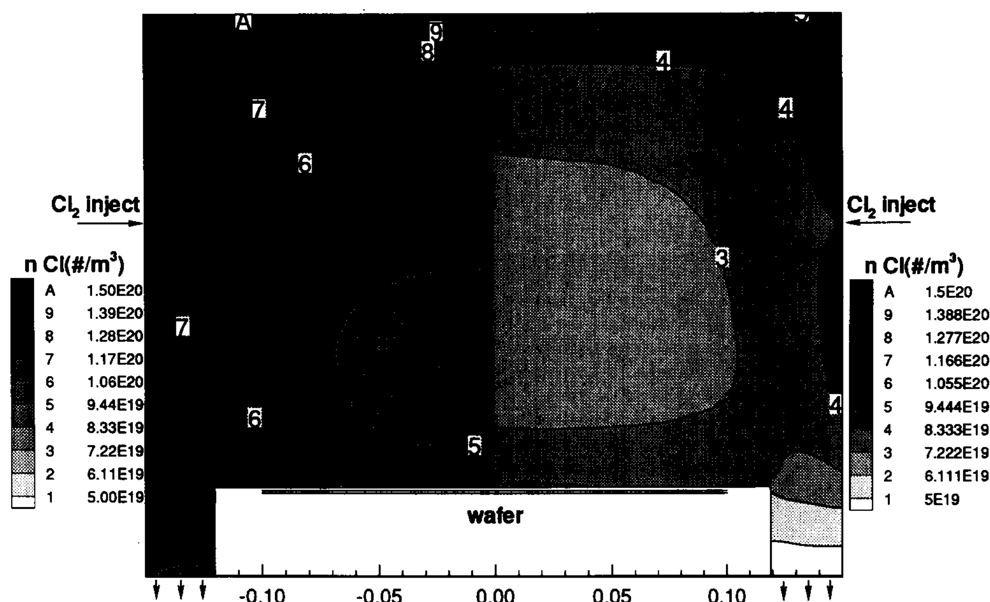

Fig. 3. (Left) Atomic chlorine number density distribution for the case of neutral etching and for a recombination probability of Cl atoms on all nonwaferwalls equal to $\gamma = 0.0082$. (Right) As in left but with $\gamma = 0.1$.

power input to the system results in a high degree of gas dissociation and a concomitantly high Cl atom density. The Cl mole fraction (not shown) ranges from ~ 0.70 near the wafer surface, to > 0.85 in the upper part of the reactor. The Cl density increases towards the reactor walls due to neutralization of Cl^+ ions (ion pumping), and the gas temperature being higher at the reactor center. The Cl atom density is lower near the wafer surface where Cl is consumed by etching (reaction probability $= 0.1$). The Cl atom density gradient along the wafer is clearly seen. Also, it is of interest to note the locally high Cl atom density over the surface surrounding the wafer ($z = 0$ m, $r = 0.10$–0.12 m). This is due to the lower reaction probability of Cl on this ring-shaped surface. This local loading effect has been studied in connection with relatively high pressure, capacitively-coupled plasma reactors [26].

The case of wall recombination probability of Cl atoms on the nonwafer surfaces $\gamma = 0.1$ is shown in Fig. 3, right. As expected, the Cl atom density (and mole fraction) is lower compared to Fig. 3, left. There is still an increasing Cl density from the reactor center towards the walls. However, the density gradients are not as strong as in Fig. 3, left. This is because the wall is now a stronger sink of Cl atoms ($\gamma = 0.1$ versus 0.0082), and this counterbalances the Cl atom build up near the walls due to ion pumping and gas heating. In fact, the Cl concentration distribution pattern can be reversed (higher density at the center) if the walls are reactive enough (higher values of γ). From the etching point of view, the Cl density over the wafer is now much more uniform as compared to Fig. 3, left. Finally, the Cl atom density is lowest in the annular region of the reactor exit where gases are pumped out.

Fig. 4 shows the molecular chlorine density corresponding to Fig. 3. Molecular chlorine is highly dissociated with a correspondingly lower density compared to Cl. Cl_2 is concentrated near the injection port and at the upper corner of the reactor where recombination of Cl atoms is more effective due to the locally higher surface-to-volume ratio. Also, a higher Cl atom recombination coefficient on the walls results in higher levels of molecular chlorine in the reactor (Fig. 4 right versus left). It is interesting to note the rather strong concentration gradients of Cl_2 along the wafer platen in Fig. 4, right.

Fig. 5 shows the silicon dichloride etch product for the case of neutral etching (left) and ion etching (right). The product density distribution is as expected; maximum at the source on the wafer surface and lower further up in the reactor. Sweeping of the product by gas flow to the exhaust port is also evident. The mole fraction of the product is quite appreciable, especially near the wafer where $SiCl_2$ accounts for almost 30% (molar) of the total gas (Fig. 5, left). Despite the relatively low pressure, strong density gradients can still be sustained. Under the present conditions chemical etching is faster than ion etching and the product concentration is correspondingly higher. Also, a "pocket" of product seems to be trapped at the upper part of the reactor where the gas is almost stagnant. Gas injection from the roof of the reactor would disrupt that relatively stagnant region.

Fig. 6 shows the Cl^+ (left) and ${Cl_2}^+$ (right) ion density distributions in the reactor, for the case of Cl recombination probability on all nonwafer walls $\gamma = 0.0082$. The Cl^+ ion density peaks off axis near the maximum of the ionization rate; it is an order of magnitude lower near the wafer surface as the space charge fields extract the ions towards the walls. In general, the ion density distribution in the reactor is mainly a function of power, pressure and reactor aspect ratio (radius/height). High values of these quantities favor off axis maxima; low values favor maxima on axis. However the ion flux on the wafer does not necessarily follow the same profile as the ion density in the bulk plasma. In fact, the ion flux shows a peak on axis under the conditions studied (see Figs. 7–9). The molecular ion density profile shown on the right side of Fig. 6 shows maxima near the gas inlet where the molecular chlorine gas also has a maximum density (see Fig. 4). Since Cl_2 is much less populous than Cl, the corresponding ion

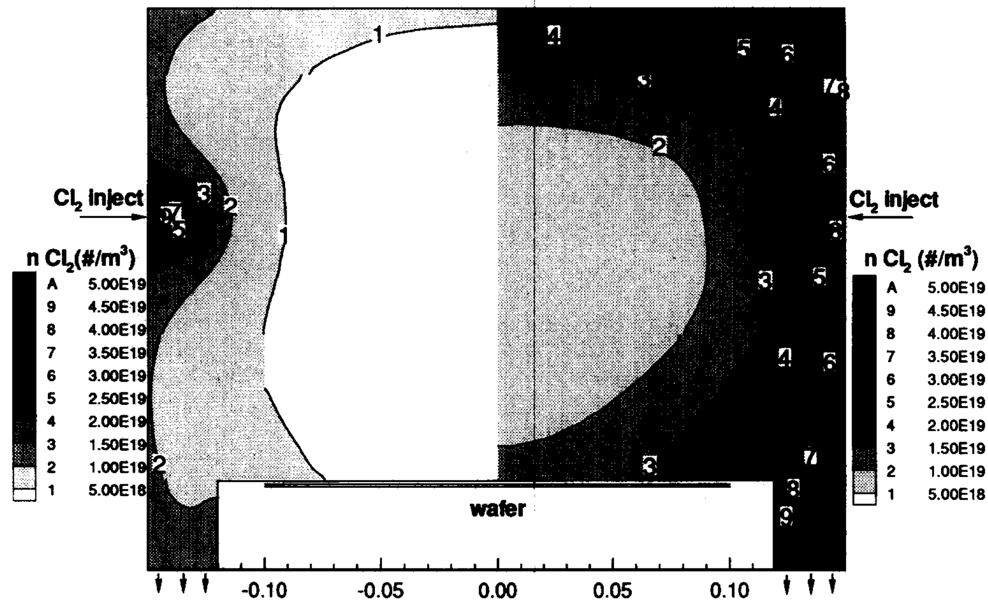

Fig. 4. Molecular chlorine number density distribution for the corresponding cases shown in Fig. 3.

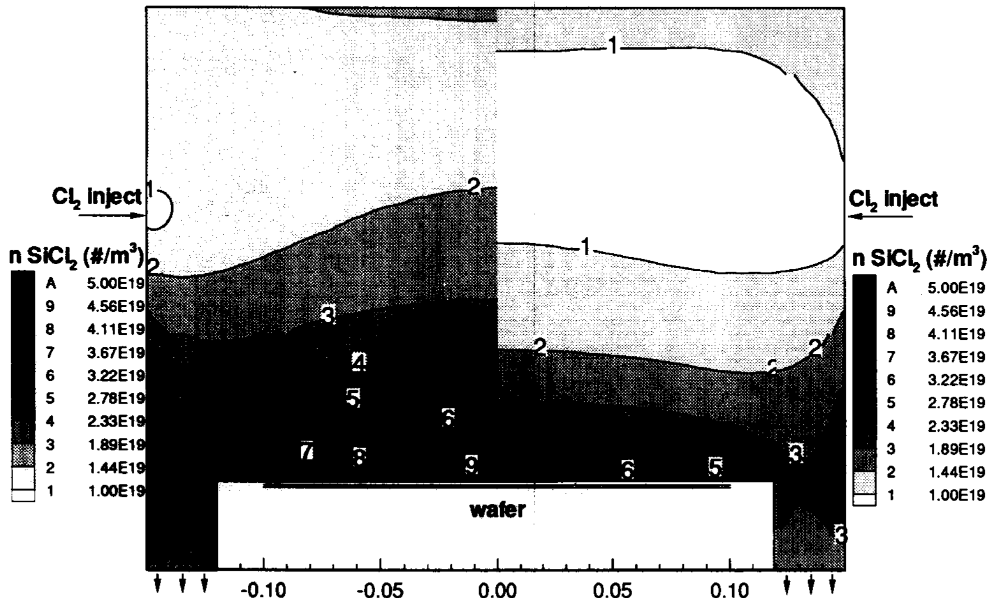

Fig. 5. (Left) Silicon chloride product distribution for the case of neutral etching and for a recombination probability of Cl atoms on all nonwafer walls equal to $\gamma = 0.0082$. (Right) As in left but for the case of ion etching. In both cases, strong concentration gradients areevident despite the low operating pressure (~10 mtorr nominal).

densities follow suit. Under these conditions, the Cl_2^+ ion flux to the wafer is highest at the wafer edge. However, the Cl_2^+ flux is too low compared to that of Cl^+ to influence the etch rate profiles on the wafer. Negative Cl^- ions (not shown) pooled near the maximum of the plasma potential (near the maximum of the Cl^+ density). Their density was extremely low near the walls.

The (overall) translational temperature was highest (~600 K) in the bulk plasma and lowest near the walls which are kept at a constant temperature of 325 K (except for the wafer which is at 375 K). The gas is heated mainly by collisions with energetic ions, by the Frank Condon effect which creates translationally hot neutrals upon dissociation of molecular chlorine (reaction 1 in Table II), and by hot neutrals created as a result of dissociative recombination (reactions 5, 7, and 8). The rarefied nature of the flow was apparent by the dramatic difference between the gas temperature near the walls and the much lower wall temperature (temperature jump can be >100 K). If the flow were in the "continuum" regime, these temperatures would be identical. The nonequilibrium nature of the flow was also seen by comparing the translational temperature of Cl_2 with the overall translational temperature; the molecular gas was more than 100 K colder in the inlet jet (the gas entered at 256 K). The flow is clearly not in equilibrium.

The radial profiles across the wafer surface of the fluxes of Cl atoms (impinging), $SiCl_2$ product (outcoming) and Cl^+ ions (impinging) are shown in Figs. 7–9. Fig. 7 shows the case

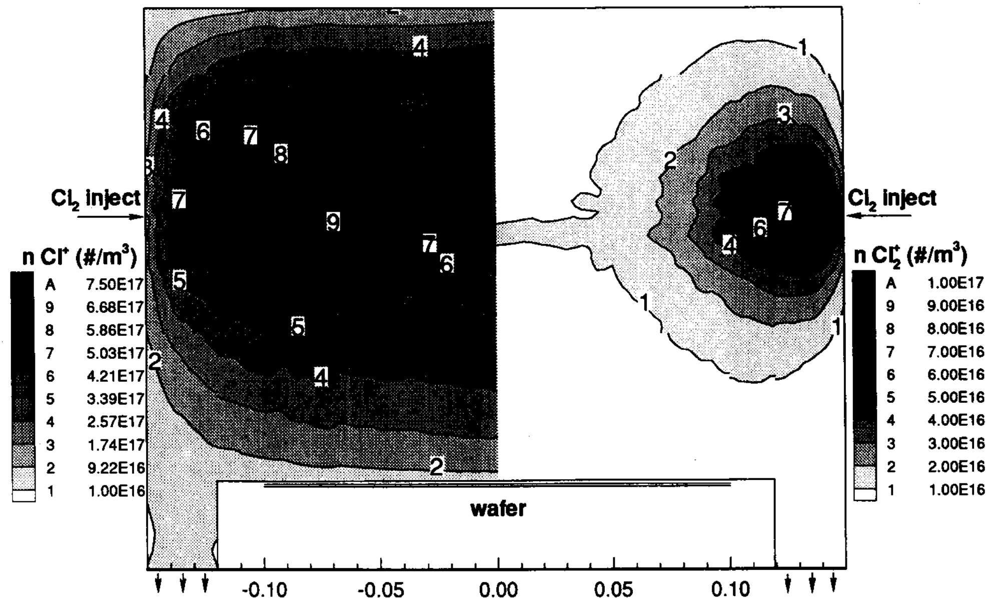

Fig. 6. (Left) Atomic chlorine ion distribution for the case of neutral etching and for a recombination probability of Cl atoms on all nonwafer walls equal to $\gamma = 0.0082$. Note, the off axis peak. This is near the maximum in ionization rate (not shown). (Right) Molecular chlorine ion distribution corresponding to left. The molecular ion density is highest near the inlet port where the neutral molecular chlorine density is also highest.

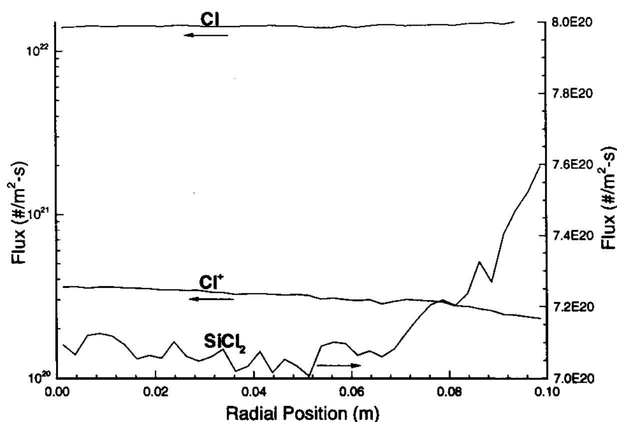

Fig. 7. Flux across the wafer radius of incoming Cl radicals and Cl^+ ions, and outgoing $SiCl_2$ etch product for the case of neutral etching and for a recombination probability of Cl atoms on all nonwafer walls equal to $\gamma = 0.0082$. Note, maximum of product flux (etch rate) at wafer edge.

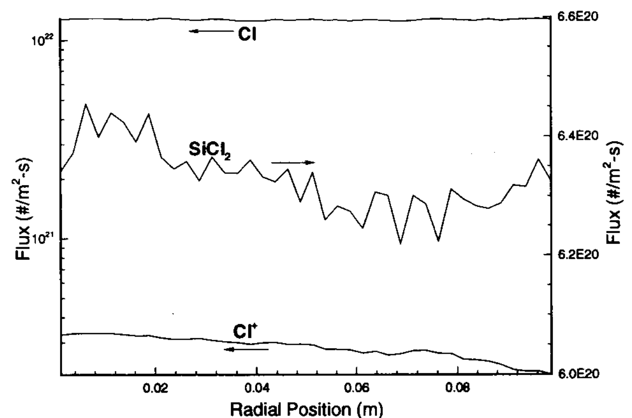

Fig. 8. As in Fig. 7 but the recombination probability of Cl atoms on the ring surrounding the wafer is $\gamma = 0.1$. Note, improved uniformity compared to Fig. 7.

of neutral etching for which the Cl recombination probability on all nonwafer walls is $\gamma = 0.0082$. For this case, the etch rate (proportional to the $SiCl_2$ flux) is maximum at the wafer edge. A $SiCl_2$ flux of 1×10^{20}% molecules/m^2-s corresponds to an etch rate 0.12 μ/min. This yields an etch rate of roughly 1 μ/min, under these conditions. The etch rate variation from center to edge is around 7%. The nonuniformity pattern of Fig. 7 would result in a bulls-eye film clearing pattern. The etch rate maximum at the edge of the wafer is due to local loading (see Fig. 3 left, and discussion associated with that figure). The etch rate can be made nearly uniform by changing the reactivity of the ring surrounding the wafer (Fig. 8). When the Cl recombination probability on this surface ($z = 0$ m, $0.10 < r < 0.12$ m and $z < 0$ m, $r = 0.12$ m) is made equal to $\gamma = 0.1$ (keeping $\gamma = 0.0082$ on all other nonwafer surfaces), the variation in etch rate is $< 1.5\%$. Fig. 9 shows the case of ion etching with a Cl recombination probability on all nonwafer walls equal to $\gamma = 0.0082$. The dominant ion is Cl^+; therefore the etch rate profile follows the Cl^+ ion flux profile. The etch rate is now maximum at the wafer center, varying by 35% between the center and edge. Note that, away from the wafer, the ion density profile has a strong off-axis maximum, yet the ion flux at the wafer has a maximum on axis. Also, the $Cl_2{}^+$ ion flux is maximum at the wafer edge but is much smaller in magnitude compared to the Cl^+ flux.

Fig. 10 shows the energy distribution of neutral Cl (solid line, upper scale) and Cl^+ ions (dashed line, lower scale) bombarding the wafer at midradius ($z = 0$ m, $r = 0.05$ m). Most of the neutrals are thermal, with a slight evidence of a tail of "hot" neutrals. Hot neutrals can be produced by the exothermic reactions 1, 5, 7, and 8 of Table II, and by charge exchange collisions. The ion energy distribution is quite broad with the maximum ion energy equal to the maximum plasma potential. Most of the ions have energies around the sheath potential ($\sim$13 V) over the grounded wafer. A small fraction

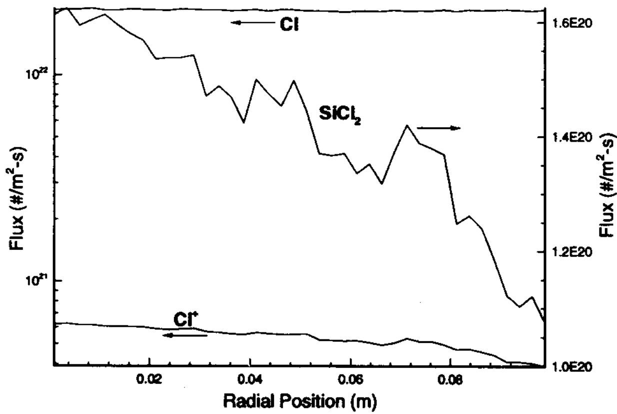

Fig. 9. Flux across the wafer radius of incoming Cl radicals and Cl^+ ions, and outgoing $SiCl_2$ etch product for the case of ion etching and for a recombination probability of Cl atoms on all nonwafer walls equal to $\gamma = 0.0082$. Note, maximum of product flux (etch rate) at wafer center, and much degraded etch uniformity compared to Figs. 7 and 8.

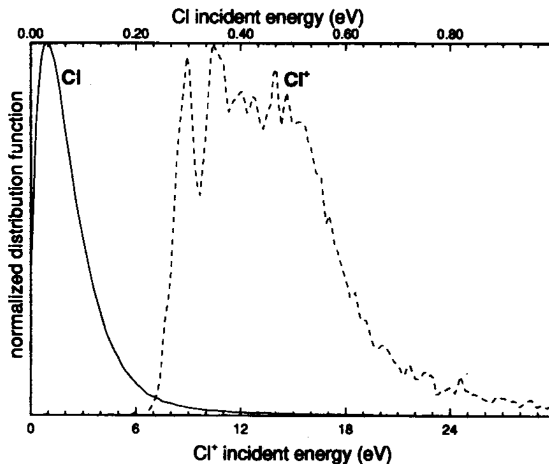

Fig. 10. Energy distribution function of Cl radicals and Cl^+ ions impinging on the wafer at the midradius, for the case of neutral etching and for a recombination probability of Cl atoms on all nonwafer walls equal to $\gamma = 0.0082$. Note, upper scale for Cl radicals.

of ions strike the wafer with only several eV of energy. These correspond to ions that have accelerated from the bulk plasma towards the wafer through the presheath and then suffered a collision to reverse their direction (moving away from the wafer). The electric field (which points towards the wafer) then brings these ions back to the wafer with only several eV energy. Clearly, one needs to apply a bias on the wafer to increase the ion bombardment energy and to straighten out any stray ions.

The angular distribution function of Cl radicals and Cl^+ ions bombarding the wafer are shown in Fig. 11. Solid lines show the distributions at the mid-radius of the wafer ($z = 0$ m, $r = 0.05$ m) dashed lines are for the wafer edge ($z = 0$, $r = 0.1$ m). As expected, the radicals are much more "thermalized" compared to the ions, although the radical angular distribution does not correspond to a perfect Maxwellian. It was found that the ions are mainly within several degrees off normal across most of the wafer surface. It is interesting to note, however, that the ion angular distribution is more spread out near the wafer edge. Also, the radical distribution is affected near the edge for the near normal incidence radicals. This behavior can be

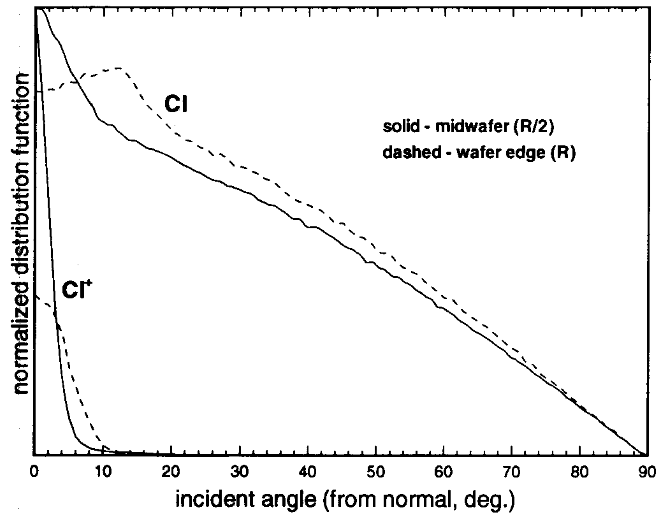

Fig. 11. Angular distribution function of Cl radicals and Cl^+ ions impinging on the wafer midradius (solid lines) and edge (dashed lines), for the case of neutral etching and for a recombination probability of Cl atoms on all nonwafer walls equal to $\gamma = 0.0082$.

explained by the fact that there is an excess of Cl neutral atoms near the wafer edge (see Fig. 3, left). Ions (mainly Cl^+) have a greater chance to charge exchange with these neutrals (charge exchange is most efficient between neutrals and daughter ions) resulting in a greater spread in the ion angular distribution. The angular and energy distributions of radicals and ions are critical information to use as input to profile evolution simulators to follow the microscopic feature sidewall profiles.

IV. Summary

A two-dimensional kinetic simulation of ion and neutral flow in an inductively coupled plasma reactor was performed using the Direct Simulation Monte Carlo (DSMC) method. Polysilicon etching with chlorine gas was studied including both gas-phase and surface chemistry. The rate coefficients for production of ions and radicals and the electrostatic field were obtained from a plasma fluid simulation. Depending on the reaction probability of Cl radicals at the reactor walls a high degree of molecular chlorine dissociation can be achieved. Cl^+ is the dominant positive ion. Ion pumping and gas heating by exothermic reactions and charge exchange results in significantly higher neutral density on the reactor walls as compared to the plasma bulk. Rather strong density gradients were sustained despite the low operating pressure (~10 mtorr nominal). The gas was not in thermodynamic equilibrium as evidenced by differences in the individual species temperatures and temperature jumps near the walls.

Two extreme conditions of reaction on the wafer surface were studied: pure neutral etching by Cl radicals and pure ion etching by Cl^+ and $Cl_2{}^+$ ions. In chemical etching, the etch rate was maximum at the wafer edge. In ion etching, the etch rate was maximum at the wafer center. The neutral etch uniformity could be made nearly perfect by adjusting the reactivity (against Cl atoms) of the ring surrounding the wafer. This demonstrates that local loading is still operative despite the low operating pressures (long mean free paths). The energy distribution function of ions bombarding the grounded wafer

was fairly broad with most ions having energy around the sheath potential. Neutrals were mostly thermal with a weak tail of "hot" neutrals resulting by plasma reactions (molecular dissociation, dissociative recombination, etc.) and/or charge exchange with energetic ions. The ion angular distribution function showed a spread of several degrees off normal. Differences in the angular distribution at the wafer midradius and at the wafer edge were observed which can have consequences for the achievable uniformity across the wafer of the shape of microscopic features etched into the wafer.

ACKNOWLEDGMENT

The authors thank S. Plimpton of SNLA for help with parallelization of the DSMC code and C. Wu of Auburn University for sending them preprints of his work prior to publication.

REFERENCES

[1] M. A. Lieberman and R. A. Gottscho, "Design of high density plasma sources for materials processing," in *Physics of Thin Films*, M. Francombe and J. Vossen, Eds. Orlando, FL: Academic, 1993.
[2] J. Hopwood, "Review of inductively coupled plasma processing reactors," *Plasma Sources Sci. Technol.*, vol. 1, pp. 109–116, 1992.
[3] J. H. Keller, J. C. Foster, and M. S. Barnes, "Novel radio-frequency induction plasma processing techniques," *J. Vac. Sci. Technol. A*, vol. 11, pp. 2487–2491, 1993.
[4] R. A. Stewart, P. Vitello, and D. B. Graves, "Two-dimensional fluid model of high density inductively coupled plasma sources," *J. Vac. Sci. Technol. B*, vol. 12, pp. 478–485, 1994.
[5] A. A. Paranjpe, "Modeling an inductively coupled plasma source," *J. Vac. Sci. Technol. A*, vol. 12, pp. 1221–1228, 1994.
[6] R. K. Porteous and D. B. Graves, "Modeling and simulation of magnetically confined low-pressure plasmas in two-dimensions," *IEEE Trans. Plasma Sci.*, vol. 19, pp. 204–213, 1991.
[7] P. L. G. Ventzek, R. J. Hoekstra, and M. J. Kushner, "Two-dimensional modeling of high plasma density inductively coupled sources for materials processing," *J. Vac. Sci. Technol. B*, vol. 12, pp. 461–477, 1994.
[8] F. Dai and C.-H. Wu, "Self-consistent multidimensional electron kinetic analysis for inductively coupled plasma sources," *IEEE Trans. Plasma Sci.*, vol. 23, no. 4, pp. 563-572.
[9] M. Surendra, "Radiofrequency discharge benchmark model comparison," *Plasma Sources Sci. Technol.*, submitted.
[10] V. Vahedi, C. K. Birdsall, M. A. Lieberman, G. DiPeso, and T. D. Rognlien, "Capacitive RF discharges modelled by particle-in-cell Monte Carlo simulation. II: Comparisons with laboratory measurements of electron energy distribution functions," *Plasma Sources Sci. Technol.*, vol. 2, pp. 273–278, 1993.
[11] C. K. Birdsall, "Particle-in-cell charged-particle simulations plus Monte Carlo collisions with neutral atoms, PIC-MCC," *IEEE Trans. Plasma Sci.*, vol. 19, pp. 65–85, 1991.
[12] G. A. Bird, *Molecular Gas Dynamics and the Direct Simulation of Gas Flows*. Oxford, UK: Oxford Science, 1994.
[13] W. L. Hermina, "Monte Carlo simulation of transitional flow around simple shaped bodies," *Proc. 15th Int. Symp. Rarefied Gas Dynamics*, 1986, vol. I, pp. 451–460.
[14] T. J. Bartel and S. J. Plimpton, "DSMC simulation of rarefied gas dynamics on a large hypercube supercomputer," Paper AIAA 92-280, presented at the 27th AIAA Thermophysics Conf., Nashville, TN, July 1992.
[15] D. G. Coronell and K. F. Jensen, "Analysis of transition regime flows in low pressure chemical vapor deposition reactors using the direct simulation Monte Carlo method," *J. Electrochem. Soc.*, vol. 139, pp. 2264–2273, 1992.
[16] A. Kersch, W. Morokoff, and C. Werner, "Selfconsistent simulation of sputter deposition with the Monte Carlo method," *J. Appl. Phys.*, vol. 75, pp. 2278–2285, 1994.
[17] A. M. Myers, J. R. Doyle, and D. N. Ruzic, "Monte Carlo simulations of sputter atom transport in low-pressure sputtering: The effects of interaction potential, sputter distribution and system geometry," *J. Appl. Phys.*, vol. 72, pp. 3064–3071, 1992.
[18] H. M. Urbassek and D. Sibold, "Sputtered atom transport in high-current gas discharges: A self-consistent computer simulation study," *J. Vac. Sci. Technol. A*, vol. 11, pp. 676–681, 1993.
[19] M. D. Kilgore, H. M. Wu, and D. B. Graves, "Neutral transport in high density reactors," *J. Vac. Sci. Technol. B*, vol. 12, pp. 494–506, 1994.
[20] T. Bartel, J. Payne, T. Sterk, R. Wise, D. Lymberopoulos, and D. Economou, "Radical and ion flux uniformity in a low pressure inductively coupled plasma reactor predicted by the direct simulation Monte Carlo method," presented at Int. Conf. Plasma Sci., Santa Fe, NM, June 1994, Paper 2C3.
[21] C. Borgnakke and P. S. Larsen, "Statistical collision model for Monte Carlo simulation of polyatomic gas mixtures," *J. Comp. Phys.*, vol. 18, pp. 405–420, 1975.
[22] S. C. Deshmukh and D. J. Economou, "Remote plasma etching reactors: Modeling and experiment," *J. Vac. Sci. Technol. B*, vol. 11, pp. 206–215, 1993.
[23] C. C. Cheng, K. V. Guinn, V. M. Donnelly, and I. P. Herman, "*In-situ* pulsed laser-induced desorption studies of the silicon chloride surface layer during silicon etching in high density plasmas of Cl_2 and Cl_2/O_2 mixtures," *J. Vac. Sci. Technol.*, to appear.
[24] D. C. Gray, V. Mohindra, and H. H. Sawin, "Redeposition kinetics in fluorocarbon plasma etching," *J. Vac. Sci. Technol. A*, vol. 12, pp. 354–364, 1994.
[25] D. P. Lymberopoulos and D. J. Economou, "Modeling and simulation of glow discharge plasma reactors," *J. Vac. Sci. Technol. A*, vol. 12, pp. 1229–1236, 1994.
[26] D. J. Economou, S.-K. Park, and G. Williams, "Uniformity of etching in parallel plate plasma reactors," *J. Electrochem. Soc.*, vol. 136, pp. 188–198, 1989.

Demetre J. Economou, for a photograph and biography, see this issue, p. 502.

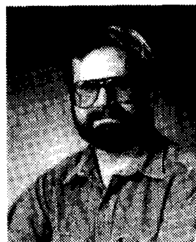

Timothy J. Bartel received the B.S. and M.S. degrees in mechanical engineering from the University of Texas, Austin and the Ph.D. degree in nuclear engineering and engineering physics from the University of Wisconsin, Madison, in 1976, 1978, and 1987, respectively.

He has worked at Sandia National Labs, Albuquerque from 1978 to 1982 and from 1987 to the present. His research interests include noncontinuum and continuum computational fluid dynamics using both PDE and particle methods, parallel computing algorithms, modeling and simulation of plasma systems, contaminant particulate transport, space-based systems, and other low gas density applications. He is the author of over a dozen publications in these areas.

Dr. Bartel is a member of the American Society of Mechanical Engineers, and the American Institute of Aeronautics and Astronautics.

Richard S. Wise was born February 28, 1967, in Philadelphia, PA. He received the B.S. degree from the University of Delaware, Newark, and the M.S. degree from the University of South Carolina, Columbia, both in chemical engineering, in 1988 and 1992, respectively. He is pursuing the Ph.D. degree at the University of Houston, Houston, TX

Prior to pursuing graduate studies, he joined the DuPont Corporation in South Carolina, where he worked on corrosion control systems and process engineering. At the University of Houston, he has focused on plasma simulation using fluid, particle, and hybrid approaches.

Dimitris P. Lymberopoulos, for a photograph and biography, see this issue, p. 580.